medRxiv preprint doi: https://doi.org/10.1101/2022.03.09.22271906; this version posted March 10, 2022. The copyright holder for this preprint
(which was not certified by peer review) is the author/funder, who has granted medRxiv a license to display the preprint in perpetuity.
It is made available under a CC-BY-NC-ND 4.0 International license .

Idetification of *CACNA1B* (p.K567R) mutation responsible for familiar AVNRT

Rong Luo[1#], Xin Cao[2#], Chenqing Zheng[3#], Jichang Huang[1#], Mingjiang Liu[4], Tao He[4], Panpan Jiang[3], Xu Yang[5], Zhenglin Yang[6], Xiushan Wu[7], Xiaoping Li[4*]

1 Institute of Geriatric Cardiovascular Disease, Chengdu Medical College, Chengdu, People's Republic of China

2 School of Acupuncture-Moxibustion and Tuina, Chengdu University of Traditional Chinese Medicine, Chengdu, China

3 Shenzhen Aone Medical Laboratory Co., Ltd., Shenzhen, China

4 Department of Cardiology, Hospital of the University of Electronic Science and Technology of China and Sichuan Provincial People's Hospital, Chengdu, Sichuan, China

5 Shenzhen RealOmics (Biotech) Co., Ltd., Shenzhen, China

6 The Sichuan Provincial Key Laboratory of Human Disease Study, Institute of Laboratory Medicine, Sichuan Provincial People's Hospital, University of Electronic Science and Technology of China, Chengdu, China

7 The Center for Heart Development, Hunan Normal University, Changsha, Hunan, China

#, These authors contributed equally to this work.

*, Authors for correspondence. Email: lixiaoping0119@163.com.

Abstract

NOTE: This preprint reports new research that has not been certified by peer review and should not be used to guide clinical practice.

medRxiv preprint doi: https://doi.org/10.1101/2022.03.09.22271906; this version posted March 10, 2022. The copyright holder for this preprint
(which was not certified by peer review) is the author/funder, who has granted medRxiv a license to display the preprint in perpetuity.
It is made available under a CC-BY-NC-ND 4.0 International license .

Atrioventricular nodal reentry tachycardia (AVNRT) is the most common form of paroxysmal supraventricular tachycardia (PSVT). The exact cause of AVNRT has not yet been found. However, an increasing number of reports suggest that AVNRT is hereditary, but no precise pathogenic gene has been found so far. In our study, we found that a point mutation of *CACNA1B* (p.K567R) which encoded the α1 subunit of N-type calcium channel (Cav 2.2), was cosegregated with AVNRT in one family. Previous research showed that overexpression and point mutations of human *CACNA1B* in zebrafish embryos may be related to abnormal heart rate. Telemetric ECG recordings showed that rats with a *CACNA1B* point mutation displayed sporadic supraventricular tachycardia and altered QRS complex morphology. In addition, the *CACNA1B* (p.K567R) rats presented a double path phenomenon and AVNRT induction by intracardiac electrophysiological examination. Indexes of heart rate variance in *CACNA1B* mutation rats showed an in cardiac sympathetic activity and an imbalance of cardiac sympathetic and parasympathetic activity. Single-cell RNA sequencing indicated that the number of neurons in the superior cervical ganglion (SCG) of mutant rats was higher than in wild-type (WT) rats, accompanied by an increased expression of *CACNA1B*. Functional enrichment in SCG proteomics suggests that point mutant rats have abnormalities in synaptic function and ion transport, which could lead to the release of neurotransmitters. This could affect the cardiac autonomic neural activity and lead to an imbalance in sympathetic and parasympathetic activity and the subsequent occurrence of AVNRT. Our findings indicate that *CACNA1B* (p.K567R) is the pathogenic gene of AVNRT in familial AVNRT and confirm that *CACNA1B* is the first definitive AVNRT pathogenic gene that has been discovered.

Key Words: AVNRT; N-type calcium channel; autonomic nervous system; parasympathetic; sympathetic

Introduction:

medRxiv preprint doi: https://doi.org/10.1101/2022.03.09.22271906; this version posted March 10, 2022. The copyright holder for this preprint
(which was not certified by peer review) is the author/funder, who has granted medRxiv a license to display the preprint in perpetuity.
It is made available under a CC-BY-NC-ND 4.0 International license .

Atrioventricular nodal reentrant tachycardia (AVNRT) is a common arrhythmia, which along with atrioventricular (AV) reentry tachycardia (AVRT), belongs in the group of paroxysmal supraventricular tachycardias (PSVT). AVNRT is considered to be caused by the reentry in the fast and slow dual pathways, which can be successfully treated with radiofrequency catheter ablation (RFCA). The precise anatomic structures that constitute the reentrant circuit and its origin are not fully understood [1-3]. In recent years, evidence was found that genetic factors may be involved in AVNRT since family aggregation of AVNRT has been discovered [4-10]. People with a family history of AVNRT have a 3.6 times higher risk than the general population to develop the condition [4]. The first reported case of familial AVNRT occurrence of was in 2001 [5]. In 2004, Hayes et al. reported familial AVNRT [6], and in 2006, Frisch et al reported two siblings with AVNRT [7]. In 2013, AVNRT was confirmed in two identical twin patients, for whom a strong case for hereditary etiology was established [8]. In 2015, Stec et al. reported the largest cohort of familial AVNRT in the world, with a total of 6 AVNRT patients [9]. In 2017, 24 AVNRT families were reported in Europe [8]. Recently, we reported 8 familial AVNRT cases in China [10]. The *PRKAG2* gene has been proven to be a possible cause of AVRT, establishing a conclusive proof of genetic basis for a PSVT subtype [11-13]. However, much less is known about a potential hereditary component in the development of AVNRT.

To the best of our knowledge, no pathogenic genes for AVNRT have been reported so far. Laura et al. [14] sequenced 67 known pathogenic genes associated with arrhythmia from 298 AVNRT patients in 2018 and found mutations in genes encoding various Na^+ and Ca^{2+} channels. These results suggested that AVNRT development is related to various ion channel dysfunctions. We used whole exome sequencing (WES) to detect mutations in 82 patients with AVNRT and found that AVNRT was closely related to gene mutations involved in ion channels, autonomic nervous system, neurotransmitter release and cardiac contraction [15]. In the present study, we additionally screened a new pathogenic gene candidate, *CACNA1B*, which encodes the α1 subunit of the N-type calcium channel (NCC) in familial AVNRT.

NCC belongs to the voltage-dependent Ca^{2+} channels (VDCCs) group. VDCC is a complex of the α1 subunit and the auxiliary α2/δ, β, and γ subunits. Molecular biology

medRxiv preprint doi: https://doi.org/10.1101/2022.03.09.22271906; this version posted March 10, 2022. The copyright holder for this preprint
(which was not certified by peer review) is the author/funder, who has granted medRxiv a license to display the preprint in perpetuity.
It is made available under a CC-BY-NC-ND 4.0 International license .

studies have revealed that α1 subunits are encoded by at least 10 distinct genes, and that *CACNA1B* encodes the α1B (Cav2.2) in NCC [16]. Different molecular combinations of the main α1 subunit determine the "type" of VDCC (L-, N-, P-, Q-, R-, and T-) [17, 18]. The NCC (Cav2.2) is largely restricted to peripheral and central neurons and plays an essential role in a variety of neuronal functions, including neurotransmitter release from sympathetic nerve terminals [17-19]. As demonstrated in N-type-deficient mice, NCC has a stronger effect on sympathetic than on parasympathetic activity, the positive inotropic response mediated by the sympathetic nervous system was dramatically decreased in N-type-deficient mice, whereas the negative inotropic response mediated by parasympathetic neurons was nearly intact in comparison with normal mice [20].

AV node conduction is heavily regulated by autonomic tonus, and the autonomic nervous system is known to play an important role in the triggering and termination of AVNRT and AVRT [21-24]. Sympathetic stimulation is commonly used to facilitate the induction of AVNRT and AVRT [21, 22], whereas enhancing the vagal tone with pharmacological or physical maneuvers is commonly used to terminate tachycardias [23, 24]. Therefore, both sympathetic and parasympathetic activities are related to the occurrence of AVNRT.

We investigated the relationship between the *CACNA1B* (p.K567R) point mutation and the imbalance of cardiac autonomic nerve activity. By using the rat model for the *CACNA1B* (p.K567R) point mutation, we found that the mutation is a gain-of-function mutation. By enhancing the sympathetic activity and inducing an imbalance between cardiac sympathetic and parasympathetic activity, a point mutation of *CACNA1B* (p.K565R) induced the occurrence of AVNRT.

Material and methods

The proband and his consanguine family members were recruited in 2017. In total, we included 82 sporadic AVNRT patients who were hospitalized at the Cardiology Department of Sichuan People's hospital from 2014 to 2017. All patients underwent a twelve-lead electrocardiogram (ECG), echocardiography, and invasive electrophysiological study (EPS). Dual atrioventricular (AV) node physiology was defined as a ≥ 50 ms increment in the atrial-His (AH) interval after a 10 ms decrement

medRxiv preprint doi: https://doi.org/10.1101/2022.03.09.22271906; this version posted March 10, 2022. The copyright holder for this preprint
(which was not certified by peer review) is the author/funder, who has granted medRxiv a license to display the preprint in perpetuity.
It is made available under a CC-BY-NC-ND 4.0 International license .

interval during the single atrial extrastimulation or a ≥ 50 ms increment in the AH interval after the pacing cycle length (CL) was shortened by 10 ms. This study was approved by the Institutional Research Committee of Sichuan Provincial People's Hospital. Written informed consent was obtained from all subjects.

Animal model

The rat model of AVNRT was created in Gem-Pharmatech (Co., Ltd, Nanjing, China) using CRISPR-Cas9 to engineer the missense mutation, *CACNA1B* (c.1700A>G/p.K567R), which leads to the p.K565R protein in rats. The genotype of each animal was confirmed via quantitative PCR. Heterozygotic, homozygotic, and WT littermates weighing 400–700 g were used for the experiments. The rats were housed at a constant temperature (23 ± 1°C) under a 12/12 h light-dark cycle, with free access to food and water. All procedures were approved by the Ethics Committee for Animal Care and Use in Chengdu Medical College, China.

Electrophysiological programmed stimulation

Briefly, the rats were anesthetized with ethyl carbamate (Mylan Seiyaku, Osaka, Japan). Lead II ECG was recorded with subdermal electrodes placed in the limbs. The right femoral vein was cannulated for saline infusion and the right femoral artery was punctured to monitor the blood pressure. The right jugular vein was cannulated to position an electrode catheter (3F, inter-electrode distance of 4 mm, SMC-304; Physio-Tech, Kiel, Germany) into the right atrium. A stimulator (SEN-8203; Jingjiang, Chengdu, China) with rectangular pulses (with 2 - 3 times the diastolic threshold voltage and 3-ms width) was used for programmed stimulation. The atrial effective refractory period (ERP) was measured with a train of eight beats (S1) of basic CLs at 150 (ERP [CL120 ms]) and 120 (ERP [CL120 ms]) followed by an extra stimulus (S2). The ERP was defined as the shortest S1S2 interval that captured the atrium and ventricles. The Wenckebach cycle length (WCL) was measured by decreasing the stimulation CL by 1-ms steps after every four stimuli until atrioventricular block (AVB) occurred. The presence or absence of dual AV node physiology (DAVNP) was defined by a ≥ 15 ms increase in A2H2 in response to a 10-ms decrease in the S1S2 interval.

Electrocardiogram measurements with biotelemetry

Surgery was performed aseptically on wild, heterozygotic, and homozygotic rats

medRxiv preprint doi: https://doi.org/10.1101/2022.03.09.22271906; this version posted March 10, 2022. The copyright holder for this preprint
(which was not certified by peer review) is the author/funder, who has granted medRxiv a license to display the preprint in perpetuity.
It is made available under a CC-BY-NC-ND 4.0 International license .

anesthetized with pentobarbital sodium (40 mg/kg). A catheter attached to a transmitter (Data Sciences International, St. Paul, MN, United States) was inserted into the abdominal wall for ECG monitoring, and the body of the transmitter was implanted in the abdominal cavity. The rats were housed individually and inspected daily for motor activity, signs of infection, and food and water intake. ECGs of freely moving rats after two weeks of recovery were measured and analyzed with a data acquisition system (Data Sciences International). Ten minute ECGs were performed at 0, 4, 8 12, 16, 20 o'clock, and short-term heart rate variability (HRV) was assessed.

Two weeks after basal assessment, atropine at a dose of 0.5 mg/kg, metoprolol at 0.25 mg/kg, isoproterenol (ISO) at 0.25/kg and conotoxin (CTX) at 30 mg/kg were intraperitoneally injected to assess the cardiovascular response.

WES and bioinformatics analysis

To identify the candidate genes for AVNRT, we applied WES to search for potential genetic variants in a family with AVNRT. WES was performed on four members of the family (the proband, sibling, and parents of the proband). The normal human population database consisted of the Thousand Genomes Project (http://browser.1000genomes. org), ESP6500SI-V2 (http://evs.gs.washington.edu/EVS), ExAC Human Exome Integration Database (http://exac. broadinstitute.org/), and the sequencing company's internal database. All variants were annotated with ANNOVAR software (version 2014).

Functional evaluation of the mutated genes with zebrafish modes

The coding sequences of WT *CACNA1B* and mutated *CACNA1B* (c.1700A>G/p.K567R) were commercially cloned by gene synthesis and then recombined into the pXT7 expression vector under the drive of the T7 promoter (YSY, China). The mRNAs were synthesized in vitro and capped with the template of linearized pXT7-*CACNA1B* or pXT7-*CACNA1B* (c.1700A>G/p.K567R) using mMESSAGE mMACHINE T7 Ultra Transcription Kit (Invitrogen, Waltham, Massachusetts, USA). The capped mRNA was further tailed using Poly(A) Tailing Kit. The capped and tailed mRNAs were purified with the MEGAclear Transcription Clean-Up Kit (Invitrogen, Waltham, Massachusetts, USA). MRNAs of WT *CACNA1B* and *CACNA1B* (c.1700A>G/p. K567R) were prepared as 100 ng/μl with RNase free nanopure water and microinjected into the zebrafish embryos (TU strain) at 1-cell stage. The amount of

medRxiv preprint doi: https://doi.org/10.1101/2022.03.09.22271906; this version posted March 10, 2022. The copyright holder for this preprint
(which was not certified by peer review) is the author/funder, who has granted medRxiv a license to display the preprint in perpetuity.
It is made available under a CC-BY-NC-ND 4.0 International license .

microinjection was 1 nl mRNA solution per embryo. The microinjected embryos were raised at 28 °C. Embryos that were not microinjected were used as controls. After 48 or 72 hours post-fertilization (hpf), 20 embryos from each group were randomly selected for heart rate measurement.

Single-cell RNA sequencing

Single-cell sequencing of the superior cervical ganglion (SGC) was described in previous studies [25]. Briefly, single cells were captured in droplet emulsions using the GemCode Single-Cell Instrument (10x Genomics, Pleasanton, California, USA), and scRNA-seq libraries were constructed as per the 10x Genomics protocol using GemCode Single-Cell 3′ Gel Bead and Library V3 Kit (10x Genomics, Pleasanton, California, USA). Raw sequencing data were demultiplexed, aligned, and counted with Cell Ranger pipelines. Cellranger mkfastq command was used to generate fastq files, which were later leveraged by the cellranger count command in order to produce expression data at a single-cell resolution. Cellranger aggr command combined sequencing data from multiple libraries with mapped sequencing depth. Pandas (v.1.1.2), NumPy (v.0.25.2), Anndata (v.0.6.19), Scanpy (v.1.8), [26] and Python (v.3.7) were used for pooling multi-sample single-cell counts and for downstream analyses. Total cells were filtered for counts (500 < n_counts < 50000), genes (300 < n_genes < 10000), mitochondrial genes (percent_mito < 20%), and ribosomal genes (percent_ribo < 20%). After filtering, gene expression for each cell was normalized (normalize_per_cell: counts_ per_cell_after = 10,000) and log-transformed (log1p). Highly variable genes were detected (detect(highly_variable_genes)) and PCA was performed based on highly variable genes (top3000). Umap dimensionality reduction and Leiden clustering (resolution 0.1 – 1.2) were carried out, and cell lineages were annotated on the basis of algorithmically defined marker gene expression for each cluster (sc.tl.rank_genes_groups, method='wilcoxon'). To aid with the annotation of the subpopulations of each cell compartment, we calculated the differentially expressed genes using the Wilcoxon Rank Sum test with Bonferroni–Hochberg adjustment as it was implemented in the scanpy workflow (log2FC > 1 and adjust p-value < 1e-05). Enrichment analyses of these genes were performed using the gene ontology enrichment tool and the Kyoto Encyclopedia of Genes and Genomes (KEGG) pathway analysis using Enrichr [27].

medRxiv preprint doi: https://doi.org/10.1101/2022.03.09.22271906; this version posted March 10, 2022. The copyright holder for this preprint
(which was not certified by peer review) is the author/funder, who has granted medRxiv a license to display the preprint in perpetuity.
It is made available under a CC-BY-NC-ND 4.0 International license .

Proteomic analysis

Briefly, all the SGC samples were resuspended with lysis buffer (1.5% SDS, 100 mMTris-Cl), and the supernatant was collected after homogenization and centrifugation. Proteins were precipitated with the acetone precipitation method. They were then dissolved in a solubilization buffer (8M urea, 100 mM Tris-HCl). The protein concentration was determined with the Bradford assay. Proteins were reduced, alkylated, and digested with trypsin as previously described. After reduction and alkylation, the sample was then diluted by adding 100□mM Tris-HCl to a urea concentration < 2M. Finally, the samples were digested with trypsin at a 1:50 trypsin-to-protein mass ratio for the first overnight digestion. Protease digestion was terminated with the addition of trifluoroacetic acid, and all samples were desalted using C18 Sep-Pak column (Waters Corporation, Milford, Massachusetts, USA). Peptide mixtures were labeled with the 16-plex tandem mass tag (TMT) reagents according to the manufacturer's protocol. TMT-labeled peptides were pooled and passed through a C18 Sep-Pak column. The labeled peptides were pooled with same amount each and then fractionated using Dionex UltiMate-3000 HPLC system (Thermo Fisher Scientific, Waltham, Massachusetts, USA). LC.ESI-MS/MS analysis was performed using an EASY-nLC 1200 (Thermo Fisher) coupled to a Orbitrap Exploris™ 480 mass spectrometer (Thermo Fisher) (Thermo Fisher). Raw data was processed by the MaxQuant environment (version 1.6.6), and Andromeda was used for the database search. MS/MS spectra were matched against the Rattus norvegicus UniProt FASTA database (20210721, 29,934 sequences). Parameters were set as follows: peptide mass tolerance□= 20 ppm; enzyme□=□trypsin; max missed cleavage□=□2; fixed modification: TMT161plex on lysine and N-term, carbamidomethyl (C); variable modification: oxidation (M), Acetyl (Protein N-term). Results were filtered with 1% FDR for peptide and protein level. Functional annotation and KEGG pathway analysis was performed using DAVID bioinformatics resources as described by G. Dennis et al. [28-30].

Statistical analysis

Data are presented as the mean ± S.E.M. Statistical analysis was conducted using a

medRxiv preprint doi: https://doi.org/10.1101/2022.03.09.22271906; this version posted March 10, 2022. The copyright holder for this preprint
(which was not certified by peer review) is the author/funder, who has granted medRxiv a license to display the preprint in perpetuity.
It is made available under a CC-BY-NC-ND 4.0 International license .

two-way analysis of variance (ANOVA) for comparison among multiple groups of different concentrations and times. One-way ANOVA followed by a Tukey post-hoc test was used to compare multiple groups. The t-test was used to compare two groups. A $P < 0.05$ was considered significant. Data analysis was carried out using GraphPad Prism 7 (GraphPad SoftwareInc., La Jolla, CA, United States).

Results

Clinical data and screening of candidate pathogenic genes

The four-generation family in our study included four patients who had bouts of tachycardia during the age of 20–40 years. The proband (III-1) was admitted to our hospital because of intermittent palpitations, which usually lasted for several minutes to half an hour, and terminated abruptly. During one of the attacks, PSVT was identified with ECG, and subsequent echocardiography showed a normal heart. The proband was diagnosed with AVNRT by intracardiac electrophysiological examination and then treated with RFCA (Figure 1). The patient's family history indicated that hers was a case of familial AVNRT: her parent (II-1), sibling (III-3), and relative (II-3) had AVRT. All the patients were diagnosed by EPS, were without other structural heart diseases, and were treated with RFCA without recurrence. The proband's 60s parent suffered from atrial fibrillation and the proband's sibling occasionally had paroxysmal sinus tachycardia detected with 24-hour Holter monitoring.

Whole exome sequencing and screening of candidate pathogenic genes

To explore the possible pathological genes in familial AVNRT, WES was performed on the three AVNRT patients and the proband's parent. After the relevant data had been analyzed, there were 7 candidate genes. Through literature review, functional support of animal model and mutation site verification of other patients in the family, *CACNA1B* (C.1700A >G/ P.K567R) was screened out as the candidate pathogenic gene. The patients carried a heterozygous mutation of this gene, which was inherited in an autosomal dominant pattern in the family. The missense mutation was in the locus which encoded the second transmembrane region of the α1 subunit in NCC, and the mutation caused arginine to replace the original lysine. The mutation site is highly evolutionarily

medRxiv preprint doi: https://doi.org/10.1101/2022.03.09.22271906; this version posted March 10, 2022. The copyright holder for this preprint
(which was not certified by peer review) is the author/funder, who has granted medRxiv a license to display the preprint in perpetuity.
It is made available under a CC-BY-NC-ND 4.0 International license .

conserved in the species and has not been reported as its allele frequency has not been found in many normal human databases such as the Thousand Genomes Project, ExAC Human Exome Integration Database, gnomeAD, and ESP Exome sequencing project. Algorithm prediction of functional impact suggested that it was a deleterious variant. Sanger sequencing of the patients suggested that the genotype of the mutation of *CACNA1B* (C.1700A>G/p.K567R) was coseparated with the disease phenotype in the family members (Figure 1).

Verification of two *CACNA1B* rare variants in sporadic AVNRT cases

In our previous study [15], we performed WES sequencing in 86 sporadic AVNRT cases and found three patients who carried two rare missense variants in *CACNA1B* (c.493G>A, p.Gly165Ser; c.6744G>C, p.Gln2248His), of which one *CACNA1B* (c.6744G>C, p.Gln2248His) locus was present in two of the patients. Algorithm prediction of functional impact suggested that it was a variant of unknown significance (supp Table-1). The variant *CACNA1B* (c.6744G>C, p.Gln2248His) could not be found in normal population databases including the Thousand Genomes Project, ExAC Human Exome Integration Database, gnomeAD, and ESP Exome sequencing project. These results support the hypothesis that *CACNA1B* may play a significant role in AVNRT pathogenesis.

Functional evaluation of *CACNA1B* (c.1700A>G/p.K567R) in zebrafish embryos

To evaluate whether the function of *CACNA1B* (c.1700A>G/p.K567R) is abnormal compared to WT *CACNA1B*, we microinjected the mRNAs into zebrafish embryos at the 1-cell stage. When the microinjected embryos reached 48 hpf or 72 hpf, we measured their heart rate. We found that overexpression of *CACNA1B* (c.1700A>G/p.K567R) increased the heart rate of the zebrafish embryos, suggesting that point mutation *CACNA1B* (C.1700A >G/ P.K567R) may be related to abnormal heart rate.

Compared with WT human *CACNA1B*, zebrafish with overexpressed mRNA, and non-injected controls, at the 48 h embryonic stage, the overexpression of human point mutant *CACNA1B* (C.1700A >G/ P.k567R) showed significantly abnormal expression of genes related to the cardiac adrenergic signaling pathway and myocardial contractile

medRxiv preprint doi: https://doi.org/10.1101/2022.03.09.22271906; this version posted March 10, 2022. The copyright holder for this preprint
(which was not certified by peer review) is the author/funder, who has granted medRxiv a license to display the preprint in perpetuity.
It is made available under a CC-BY-NC-ND 4.0 International license .

pathway (top 20 enriched pathways). At the 72-h embryonic stage, the expression of genes related to cardiac adrenergic signaling pathway, calcium ion signaling pathway, and myocardial contractile pathway was significantly abnormal in zebrafish with overexpression of the human point mutation *CACNA1B* (C.1700A >G/ P.K567R).

Functional evaluation of *CACNA1B* (c.1700A>G/p.K567R) in rats

The homozygous mutant rats had a normal life span of more than a year and were capable of producing offspring with a normal litter size. Echocardiography and HE staining of the heart tissue indicated normal heart morphology, structure, and function. Additionally, the ratio of heart-weight to body-weight was normal, the measurement of energy metabolism showed that the body temperature and consumption of carbon dioxide and oxygen were normal, the degree of activity had an increasing trend, and basal blood pressure increased in the awake state in heterozygotic and homozygotic mutant rats.

Telemetric ECG analysis in point mutation of *CACNA1B* rat

To reduce the interference of postoperative stress, we began evaluating ECG recordings from day 14 post-surgery. ECG of the control rats showed a regular pattern indicative of physiological pacemaking and excitation propagation. While rats with a *CACNA1B* point mutation displayed sporadic supraventricular tachycardia and atrial/junctional escape rhythm, a block similar to the 2nd degree AVB type II (Mobitz type II, 2:1 and 3:1), sometimes along with altered atrial depolarization, was indicated by negative P-waves, ventricular ectopic beats and altered morphology of the QRS complex, which was either inverted, broadened and split, or of normal width and split.

Heterozygotic and homozygotic rats showed enhanced sympathetic activity

A typical Poincare plot of the RR interval is depicted in Fig. 2A, and the heart rate in relation to time points (Fig. 2B) and HRV variables are shown in Fig. 2C-F. Heart rate tended to spike in the period between 20 to 4 o'clock in heterozygotic rats. Root mean square of successive RR interval differences (RMSSD) was lower in both heterozygotic and homozygotic rats compared to WT rats. Similarly, absolute power of the high-frequency (HF) band (0.15 – 0.4 Hz) was higher in heterozygotic and homozygotic

medRxiv preprint doi: https://doi.org/10.1101/2022.03.09.22271906; this version posted March 10, 2022. The copyright holder for this preprint
(which was not certified by peer review) is the author/funder, who has granted medRxiv a license to display the preprint in perpetuity.
It is made available under a CC-BY-NC-ND 4.0 International license .

rats than in WT rats, suggesting an increased sympathetic or decreased parasympathetic activity in heterozygotic and homozygotic mice.

ISO-induced incidence of arrhythmia and typical trace of torsades de pointes (Tdp) are shown in in Fig 2J and K. After injection of atropine, the heart rate percentage change was greater in WT than in heterozygotic rats, suggesting impairment in vagal regulation in heterozygotes. Notably, metoprolol inhibits the β receptors and decreases the heart rate; however, heart rate was increased in homozygotic rats, suggesting the dysfunction of the sympathetic nervous system (Fig. 2L-O). In the WT group, ISO caused single premature ventricular complexes (PVC) in 3 out of 6 rats and AVB in one rat (Fig. 2K). In the heterozygotic group, ISO led to the death of one rat, and induced frequent PVCs in 3 out of 6 and AVBs in 2 out of 6 rats (Fig. 2K). In the homozygotic group, ISO caused Tdp, ventricular tachyarrhythmia and AVB in one rat, and PVC in 3 out of 5 rats (Fig. 2K).

Heterozygotic rats showed AVNRT and dual AV node physiology

Representative traces of the AVNRT (Fig. 3A) and DAVNP (Fig. 3B-D) in heterozygotic rats are depicted. AVNRT was induced by EPS in a heterozygotic rat, but not in WT or homozygotic rats. In addition, a DAVNP (Figure 3B-D) was observed in 2 out of 6 WT, 5 out of 6 heterozygotic, and 5 out of 9 homozygotic rats (Table 1). No difference was observed in the other variables such as AERO, VERP, and AVNERP (Figure 3E-L).

Sc-RNA sequencing

Because the superior cervical ganglion (SCG) is the largest sympathetic ganglion in the human body and produces a cardiac nerve with which it contributes to the cardiac sympathetic activity, we chose it for single-cell RNA sequencing, in order to explore the molecular mechanism between *CACNA1B* point mutation and AVNRT in cell subsets. To characterize the full complement of cell types, following dissociation, SCG were pooled and processed on a 10X microfluidic chip, and the resulting libraries were sequenced on an Illumina HiSeq (San Diego, California, USA). After filtering out the low-quality samples, 58,084 cells were retained, an average of 1,584 unique transcripts were captured, and ~1,589 genes were detected in a typical cell.

medRxiv preprint doi: https://doi.org/10.1101/2022.03.09.22271906; this version posted March 10, 2022. The copyright holder for this preprint
(which was not certified by peer review) is the author/funder, who has granted medRxiv a license to display the preprint in perpetuity.
It is made available under a CC-BY-NC-ND 4.0 International license .

Following identification of genes with highly variable expression across the data set, we assigned cells into 8 different groups, including glial cells, neuronal cells, Schwann cells, dendritic cells, epithelial cells, endothelial cells, smooth muscle cells, and fibroblasts (Figure 4A-B). The expression of *CACNA1B* is almost entirely in the neuronal cell, and the proportion of neuronal cells in heterozygous point mutant rats was significantly higher than in wild rats. Because the SCG belongs to the sympathetic nervous system, the increase in expression of *CACNA1B* in heterozygous point mutant rats will be closely related to the release of neurotransmitters, which could then enhance the neurotransmitter activity, and in turn enhance sympathetic activity. At the same time, we also found that there were two subgroups of neurons: in the first subgroup (Neu-1) biological function enrichment in the synapses was increased in the heterozygous rat (Figure 4C-F), while in the second subgroup (Neu-2) biological function enrichment in the ion transport had a strong increase in both homozygous and heterozygous rats (Figure 4G). The synapses and ion transport all have an important role in the release of neurotransmitters from SCG neurons. They can cause changes in cardiac autonomic nerve activity, and in turn cause the occurrence of AVNRT. Pseudotime analysis found that the four cells (Neu_1, Nue_2, glial cells, and Schwann cells) have a close evolutionary relationship (Figure 4H).

At the same time, we performed single-cell sequencing of non-cardiomyocytes in the atrioventricular node tissue of point mutant rats. Compared to the superior cervical ganglion, there are far fewer neuronal cells in the AV node tissue. Due to the very small proportion of neurons, the number of neurons in point mutant and WT rats did not change significantly, but in point mutant rats, the expression of *CACNA1B* gene was significantly higher than that in WT rats as showed in Figure 4.

Proteomic analysis

To understand the function of *CACNA1B* (c.1700A>G/p.K567R) SCG at the system level, we carried out TMT-based proteomics. Briefly, SCG tissues were collected from the control (n = 4), homozygous (n = 4), and heterozygous rat (n = 5) groups and digested using the FASP method [29]. Equal amounts of the resulting tryptic peptides were labeled with TMT 16-plex reagents. The labeled peptides were pooled and fractionated by basic

medRxiv preprint doi: https://doi.org/10.1101/2022.03.09.22271906; this version posted March 10, 2022. The copyright holder for this preprint
(which was not certified by peer review) is the author/funder, who has granted medRxiv a license to display the preprint in perpetuity.
It is made available under a CC-BY-NC-ND 4.0 International license .

RPLC. Six fractions for each biological replicate were collected for LC-MS/MS analysis.

To better understand the qualitative proteomics data, differentially expressed proteins (DEPs) are shown in volcano plots based on the following criteria: fold change ratios ≥ 1.2 or ≤ 0.83 and p-value < 0.05. In total, 82 DEPs (homozygous vs. control, 45 upregulated; 37 downregulated), 59 DEPs (heterozygote vs. control, 39 upregulated; 20 downregulated), and 23 DEPs (homozygous vs. heterozygote, 11 upregulated; 12 downregulated) were acquired (Figure 5A), suggesting that the homozygous and heterozygous rats were clearly distinguished from the controls, consistent with the phenotypes of SGC in the three groups. The heatmap further confirmed these differences (Figure 5B).

To further discover the differences in proteomic changes between different groups, molecular function (MF) and KEGG enrichment were carried out. The NCC *CACNA1B* is mainly located on peripheral and central neurons and plays an essential role in neurotransmitter release at sympathetic nerve terminals [17-19]. MF enrichment related to protein binding, structural molecule activity, calcium ion binding, and metal ion binding (homozygous vs. control) (Figure 5C), and the KEGG pathway mainly related to protein digestion and absorption, ECM-receptor interaction, and axon guidance (Figure 5D), suggesting that the homozygous *CACNA1B* may play an important role in regulating calcium ion activity in axon guidance. Similar to the results of the sc-RNA sequencing, MF and KEGG enrichment in heterozygous rats related to cytosolic Ca^{2+}, chemical synapses, and neuron postsynapse (Figure 5E and F), indicating that the heterozygous *CACNA1B* may play an important role in regulating calcium ion activity in synapses, in consistence with the results in homozygous rats.

Discussion

The present study has demonstrated that familial AVNRT is caused by the mutation of the *CACNA1B* gene by simulating the clinical manifestations of AVNRT in rats with the point mutation, including the phenomenon of dual atrioventricular node pathway and the onset of typical AVNRT. From the indexes of HRV, responses to cardiac autonomic nerve blocking drugs, and the results of single-cell sequencing and proteomic analysis, we concluded that the *CACNA1B* mutation was a gain-of-function mutation. By

medRxiv preprint doi: https://doi.org/10.1101/2022.03.09.22271906; this version posted March 10, 2022. The copyright holder for this preprint
(which was not certified by peer review) is the author/funder, who has granted medRxiv a license to display the preprint in perpetuity.
It is made available under a CC-BY-NC-ND 4.0 International license .

enhancing the sympathetic activity and creating an imbalance between the sympathetic and the parasympathetic cardiac nervous system, the mutation of *CACNA1B* causes AVNRT.

Atrioventricular nodal reentry tachycardia (AVNRT) is the most common form of PSVT, accounting for over 50% of all cases [31]. Previously, two cardiac areas with diverse electrophysiological conduction properties (termed pathways) have been implicated in the reentry circuits in AVNRT patients, the fast and slow pathway [32]. Until now, no biochemical underpinnings could account for AVNRT. However, clustering of AVNRT in different families, suggested that there may be a heritable component to the occurrence of AVNRT [4-10]. Identifying possible disease-causing genes could potentially lend new insight into the pathophysiology of AVNRT and play an important role in future diagnoses and risk assessments.

Voltage-dependent Ca^{2+} channels mediate Ca^{2+} entry essential for a wide variety of physiological functions. The N-type VDCC is the high voltage-activated Ca^{2+} channel. Ca^{2+} influx through N-type channels at syntaxin and synaptotagmin, has been shown to control neurotransmitter release in a number of different neurons [17-20, 33]. ω-CgTx-GVIA, a selective inhibitor of the N-type channel, suppressed the sympathetic nerve-mediated positive inotropic effects in isolated guinea pig atria [34, 35] and blocked sympathetic cardiac efferent activity in conscious rabbits [36]. In isolated left atria prepared from N-type-deficient mice, the positive inotropic responses to electrical sympathetic neuronal stimulation were dramatically decreased compared with those of normal mice, while parasympathetic nervous activity in the mutant mice was nearly identical to that of WT mice. These results provide direct evidence that N-type VDCCs are indispensable for the function of the sympathetic nervous system in circulatory regulation [20].

AV node conduction is heavily regulated by autonomic tone. Sympathetic stimulation is commonly used to facilitate induction of PSVTs, whereas enhanced vagal tone by use of pharmacological or physical maneuvers is commonly used to create the opposite effect, since vagal enhancement can terminate the tachycardia either through the anterograde slow or the retrograde fast pathway [21-24]. However, in some patients, the onset of AVNRT occurs at times of presumed increased vagal tone. There was a marked

medRxiv preprint doi: https://doi.org/10.1101/2022.03.09.22271906; this version posted March 10, 2022. The copyright holder for this preprint
(which was not certified by peer review) is the author/funder, who has granted medRxiv a license to display the preprint in perpetuity.
It is made available under a CC-BY-NC-ND 4.0 International license .

prolongation of the anterograde relative refractory period of the fast, but not the slow pathway, indicating that the changes in electrophysiological properties are potentially proarrhythmic and can induce AVNRT [37]. Therefore, the imbalance of cardiac sympathetic activity and parasympathetic activity will induce AVNRT.

In the rats with *CACNA1B* (C.1700A > G/ P.K567R), the cardiac sympathetic activity was increased and the balance of cardiac sympathetic and parasympathetic activity was dysfunctional, as showed by the changes of HRV and response to drug administration. The pathogenic changes found were an increased number of neurons and overexpression of *CACNA1B* along with changes in synapses and ion transport as measured by sc-RNA sequencing and proteomic analysis. In conclusion, to the best of our knowledge, this is the first study that identified the mutation of *CACNA1B* (C.1700A > G/ P.K567R) as the cause of AVNRT.

Funding

This work was supported by grants from the Chinese National Natural Science Foundation (No. 81770379, 32171182, 81470521, and 81670290).

Declaration of competing interest

None

Acknowledgements

The authors would like to thank all patients who provided samples used in this study.

Reference

1. McGuire MA, Janse MJ. New insights on anatomical location of components of the reentrant circuit and ablation therapy for atrioventricular junctional reentrant tachycardia. *Curr Opin Cardiol*. 1995; 10:3-8.

2. Wu J, Zipes DP. Mechanisms underlying atrioventricular nodal conduction and the reentrant circuit of atrioventricular nodal reentrant tachycardia using optical mapping. *J*

medRxiv preprint doi: https://doi.org/10.1101/2022.03.09.22271906; this version posted March 10, 2022. The copyright holder for this preprint
(which was not certified by peer review) is the author/funder, who has granted medRxiv a license to display the preprint in perpetuity.
It is made available under a CC-BY-NC-ND 4.0 International license .

Cardiovasc Electrophysiol. 2002;13:831-834.

3. Katritsis DG, Becker A. The atrioventricular nodal reentrant tachycardia circuit: a proposal. *Heart Rhythm*. 2007;4:1354-1360.

4. Michowitz Y, Anis-Heusler A, Reinstein E, et al. Familial occurrence of atrioventricular nodal reentrant tachycardia. Circ Arrhythm Electrophysiol. 2017, 10(2): e004680.

5. Jay PY, Berul CI. Hereditary supraventricular tachycardias. In CI Berul, JA Towbin (eds.): Molecular Genetics of Cardiac Electrophysiology.Boston, Kluwer, 2001, pp. 81.

6. Hayes JJ, Sharma PP, Smith PN, Vidaillet HJ. Familial atrioventricular nodal reentry tachycardia. Pacing Clin Electrophysiol, 2004, 27(1) : 73-76.

7. Frisch DR, Kwaku KF, Allocco DJ, Zimetbaum PJ. Atrioventricular nodal reentranttachycardia in two siblings with Wolfram syndrome. J Cardiovasc Electrophysiol, 2006, 17 (2): 1029-1031.

8. Barake W, Caldwell J, Baranchuk A. Atrioventricular nodal re-entry tachycardia in identical twins: A case report and literature review. Indian Pacing Electrophysiol J, 2013, 13 (1): 45-51.

9. Stec S, Deutsch K, Zienciuk-Krajka A. The world's largest family with familial atrio-ventricular nodal reentry tachycardia. Kardiol Pol, 2015, 73 (12): 1339.

10. Chen XP, Yan C, Luo R, Zhu Y, Qian M, Liu X, Liu M, Ikeda T, Li X. Clinical report of 8 cases of familial atrioventricular nodal reentrant tachycardia from China. Kardiol Pol. 2021, 79(2):185-187.

11. Vidaillet HJ, Pressley JC, Henke E, et al. Familial occurrence of accessory pathways (preexcitation syndrome). N Engl J Med 1987; 317:65-69.

12. Gollob MH, Green MS, Tang A, et al. Identification of a gene responsible for familial Wolff-Parkinson-White syndrome. N Engl J Med 2001; 344:1823-1864.

13. Gollob MH, Seger JJ, Gollob TN, et al. Novel PRKAG2 mutation responsible for the genetic syndrome of ventricular preexcitation and conduction system disease with childhood onset and absence of cardiac hypertrophy. Circulation 2001; 104:3030-3033.

14. Andreasen L, Gustav Ahlberg G, Tang C, Andreasen C, Hartmann JP, Tfelt-Hansen J, Behr ER, Pehrson S, Haunsø S, LuCamp, Weeke PE, Jespersen T, Olesen MS, Svendsen JH. Next-generation sequencing of AV nodal reentrant tachycardia patients identifies

medRxiv preprint doi: https://doi.org/10.1101/2022.03.09.22271906; this version posted March 10, 2022. The copyright holder for this preprint
(which was not certified by peer review) is the author/funder, who has granted medRxiv a license to display the preprint in perpetuity.
It is made available under a CC-BY-NC-ND 4.0 International license .

broad spectrum of variants in ion channel genes. Eur J Hum Genet. 2018, 26(5):660-668.

15. Luo R, Zheng C, Yang H, Chen X, Jiang P, Wu X, Yang Z, Shen X, Li X. Identification of potential candidate genes and pathways in atrioventricular nodal reentry tachycardia by whole-exome sequencing. Clin Transl Med. 2020, 10(1):238-257.

16. Ertel EA, Campbell KP, Harpold MM, et al. Nomenclature of voltage-gated calcium channels. Neuron. 2000, 25:533-535.

17. Kobayashi T, Mori Y. Ca^{2+} channel antagonists and neuroprotection from cerebral ischemia. Eur J Physiol. 1998, 363:1-15.

18. Mori Y, Mikala G, Varadi G, et al. Molecular pharmacology of voltage-dependent calcium channels. Jpn J Pharmacol. 1996, 72:83-109.

19. Gasparini S, Kasyanov AM, Pietrobon D, et al. Presynaptic R-type calcium channels contribute to fast excitatory synaptic transmission in the rat hippocampus. J Neurosci. 2001, 21: 8715-8721.

20. Mori Y, Nishida M, Shimizu S, et al. Ca^{2+} Channel α1B Subunit (CaV2.2)Knockin Rat Reveals a Predominant Role of N-Type Channels in the Sympathetic Regulation of the Circulatory System. Trends Cardiovasc Med. 2002, 12: 270-275.

21. Hariman RJ, Gomes JAC, El-Sherif N. Catecholamine-dependent atrioventricular nodal reentrant tachycardia. *Circulation*. 1983;67:681-686.

22. Huycke EX, Lai WT, Nguyen NX, et al. Role of intravenous isoproterenol in the electrophysiologic induction of atrioventricular node reentrant tachycardia in patients with dual atrioventricular node pathways. *Am J Cardiol*. 1989;64:1131-1137.

23. Cohn AE, Fraser FR. Paroxysmal tachycardia and the effect of stimulation of the vagus nerves by pressure. *Heart*. 1913;93-108.

24. Wen ZC, Chen SA, Tai CT, et al. Electrophysiological mechanisms and determinants of vagal maneuvers for termination of paroxysmal supraventricular tachycardia. *Circulation*. 1998; 98: 2716-2723.

25. Haque A, Engel J, Teichmann SA, Lönnberg T. A practical guide to single-cell RNA-sequencing for biomedical research and clinical applications. Genome Med. 2017; 9(1):75.

26. Wolf FA, Angerer P, Theis FJ. SCANPY: large-scale single-cell gene expression data analysis. Genome Biol. 2018;19(1):15.

medRxiv preprint doi: https://doi.org/10.1101/2022.03.09.22271906; this version posted March 10, 2022. The copyright holder for this preprint
(which was not certified by peer review) is the author/funder, who has granted medRxiv a license to display the preprint in perpetuity.
It is made available under a CC-BY-NC-ND 4.0 International license .

27. Xie Z, Bailey A, Kuleshov MV, et al. Gene Set Knowledge Discovery with Enrichr. Curr Protoc. 2021;1(3):e90.

28. Dennis G, Jr., Sherman BT, Hosack DA, Yang J, Gao W, Lane HC, Lempicki RA. DAVID: Database for Annotation, Visualization, and Integrated Discovery. Genome Biol, 2003; 4:P3

29. Narayan V, Ly T, Pourkarimi E, Murillo AB, Gartner A, Lamond AI, Kenyon C. Deep Proteome Analysis Identifies Age-Related Processes in C. elegans. Cell Syst. 2016, 3:144-159

30. Kumar L, M EF. Mfuzz: a software package for soft clustering of microarray data. Bioinformation 2007, 2:5-7.

31. Kwaku KF, Josephson ME: Typical AVNRT-an update on mechanisms and therapy. Card Electrophysiol Rev. 2002; 6:414-421.

32. Akhtar M, Jazayeri MR, Sra J, Blanck Z, Deshpande S, Dhala A. Atrioventricular nodal reentry (AVNRT) clinical, electrophysiological, and therapeutic considerations. Circulation.1993; 88:282-95.

33. Hirning LD, Fox AP, McCleskey EW, et al. Dominant role of N-type Ca^{2+} channels in evoked release of norepinephrine from sympathetic neurons. Science.1988, 239:57-61.

34. Hong SJ, Chang CC. Calcium channel subtypes for the sympathetic and parasympathetic nerves of guinea-pig atria. Br J Pharmacol. 1995, 116:1577-1582.

35. Vega T, De-Pascual RD, Bulbena O, Garcia AG. Effects of ω-conotoxins on noradrenergic neurotransmission in beating guinea pig atria. Eur J Pharmacol. 1995, 276:231-238.

36. Pruneau D, Angus JA: ω-conotoxin GVIA, the N-type calcium channel inhibitor, is sympatholytic but not vagolytic: consequences for hemodynamics and autonomic reflexes in conscious rabbits. J Cardiovasc Pharmacol. 1990.16:675-680.

37. Chuen-Wang Chiou, Shih-Ann Chen, Ming-Ho Kung, et al. Effects of Continuous Enhanced Vagal Tone on Dual Atrioventricular Node and Accessory Pathways. Circulation. 2003; 107: 2583- 2588.

medRxiv preprint doi: https://doi.org/10.1101/2022.03.09.22271906; this version posted March 10, 2022. The copyright holder for this preprint
(which was not certified by peer review) is the author/funder, who has granted medRxiv a license to display the preprint in perpetuity.
It is made available under a CC-BY-NC-ND 4.0 International license .

medRxiv preprint doi: https://doi.org/10.1101/2022.03.09.22271906; this version posted March 10, 2022. The copyright holder for this preprint
(which was not certified by peer review) is the author/funder, who has granted medRxiv a license to display the preprint in perpetuity.
It is made available under a CC-BY-NC-ND 4.0 International license .

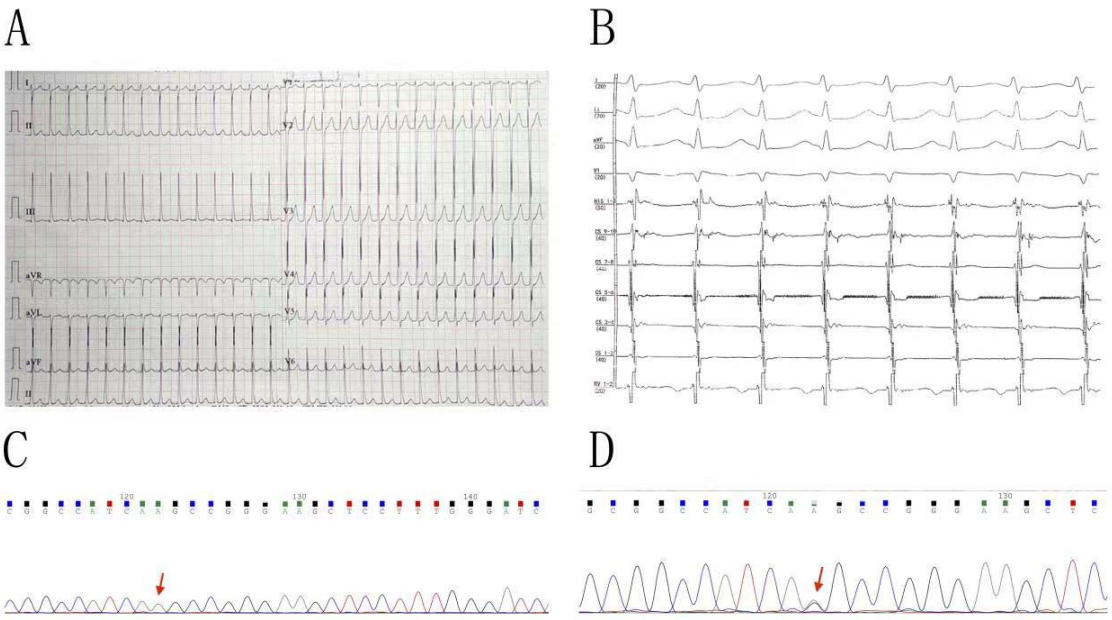

Figure 1. Clinical data of proband and first generation sequencing by Sanger method. 12 lead body surface electrocardiogram (A) and intracardiac electrocardiogram (B) during tachycardia attack; (C) First-generation sequencing map in the non-attacked familiar members; (D) First-generation sequencing map in the patients, the heterozygous mutation site in *CACNA1B* (c.1700A>G/p.K567R) was marked by red arrows.

medRxiv preprint doi: https://doi.org/10.1101/2022.03.09.22271906; this version posted March 10, 2022. The copyright holder for this preprint
(which was not certified by peer review) is the author/funder, who has granted medRxiv a license to display the preprint in perpetuity.
It is made available under a CC-BY-NC-ND 4.0 International license .

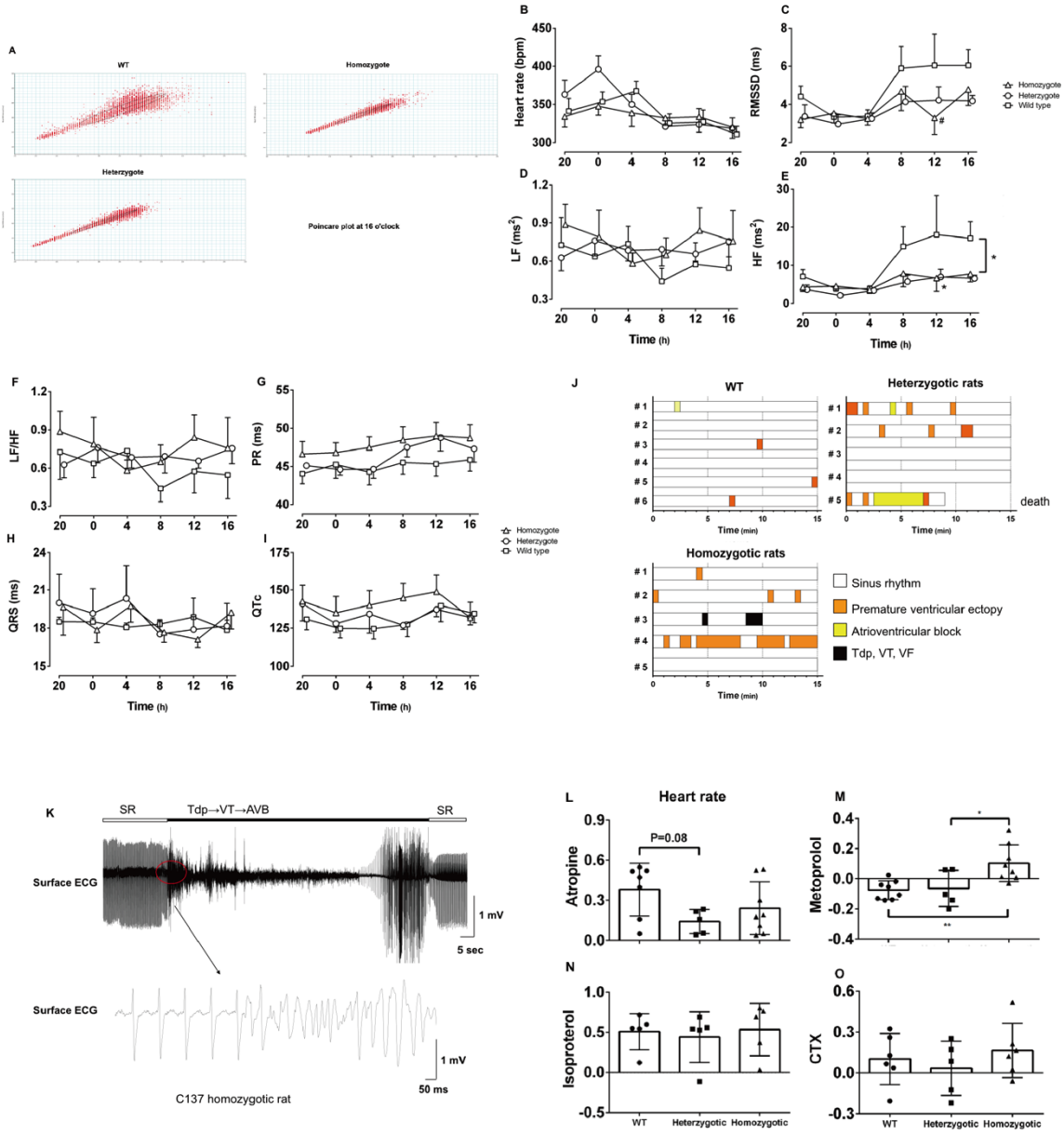

Figure 2. Electrophysiologyin conscious WT, heterozygotic and homozygotic groups. (A) Typical traces of Poincare plot of the RR interval. Ten min beats were plotted at16 o'clock in a WT, heterozygotic and homozygotic rat. (B-I) Time course of heart rate, root mean square of successive RR interval differences (RMSSD), absolute power of the low-frequency band (LF), absolute power of the high-frequency band (HF), LF/HF, PR interval, QRS width and QTc (corrected QT (QTc) interval was calculated with the modified Bazett's formula) in WT (square), heterozygotic (circle) and homozygotic (tringle) rats. (J) Summary of isoproterenol-induced arrhythmia in the WT, heterozygotic and homozygotic rats. Each column indicates the onset of arrhythmia in each rat. The

medRxiv preprint doi: https://doi.org/10.1101/2022.03.09.22271906; this version posted March 10, 2022. The copyright holder for this preprint
(which was not certified by peer review) is the author/funder, who has granted medRxiv a license to display the preprint in perpetuity.
It is made available under a CC-BY-NC-ND 4.0 International license .

columns are marked according tothe severity of arrhythmias developed each 30 second. Black column: the occurrence of torsades de pointes (Tdp), ventricular tachycardia (VT). Orange column: the occurrence of premature ventricular complex (PVC). Yellow column: the occurrence of atrioventricular block (AVB). (K) Typical trace of Tdp in a hemozygotic rat. (L-O) Heart rate in response to atropine, metoprolol isoproterenol (ISO) and conotoxin (CTX) in WT, heterozygotic and homozygotic rats. Data are presented as the mean ± S.E.M. Asterisks indicate statistically significant difference by $P < 0.05$. SR: sinus rhythm.

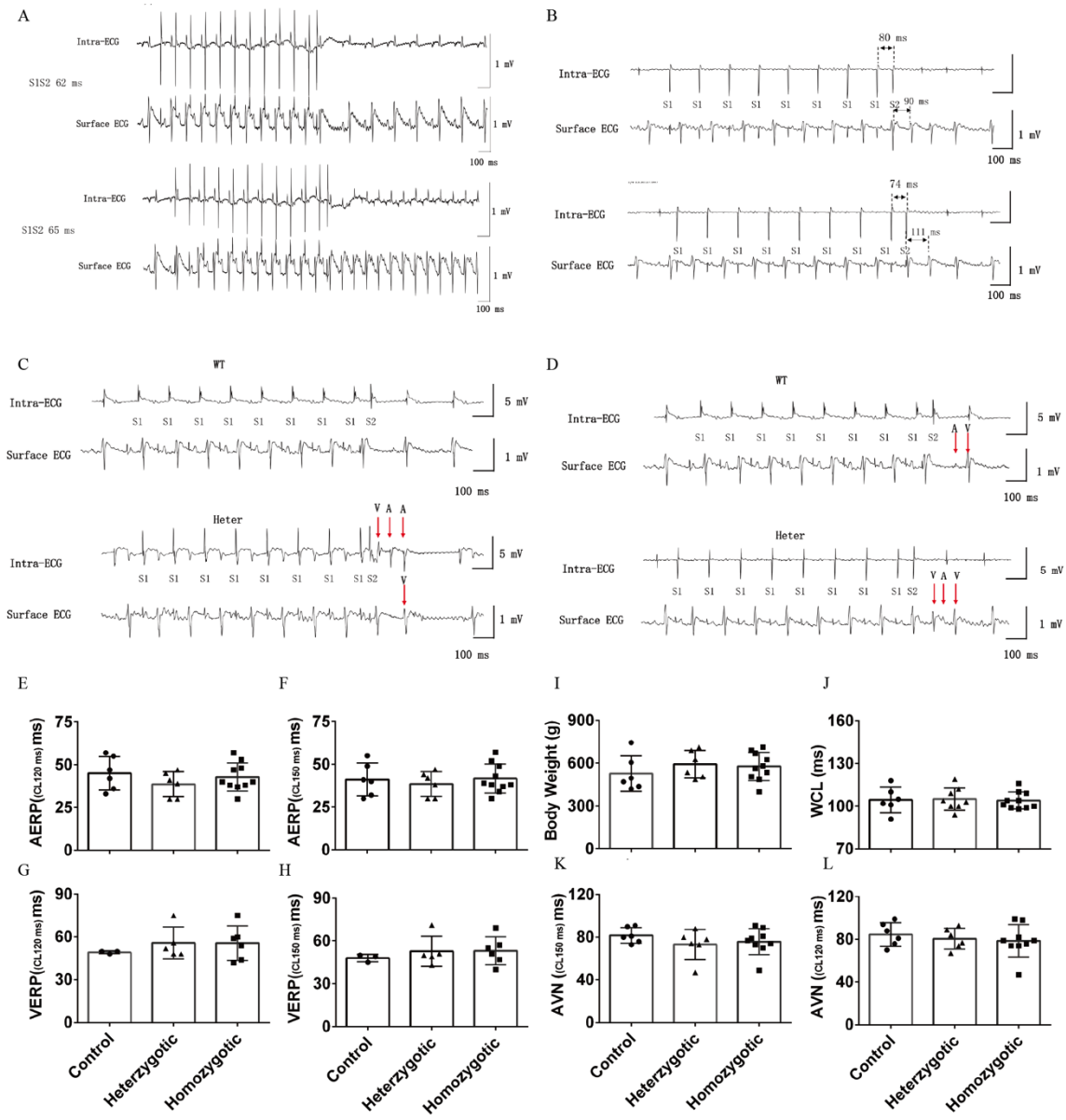

medRxiv preprint doi: https://doi.org/10.1101/2022.03.09.22271906; this version posted March 10, 2022. The copyright holder for this preprint
(which was not certified by peer review) is the author/funder, who has granted medRxiv a license to display the preprint in perpetuity.
It is made available under a CC-BY-NC-ND 4.0 International license .

Figure 3. Electrophysiology by programmed stimulation in anaesthetized WT, heterozygotic and homozygotic groups. (A-D) Typicaltrace of AVNRT and a dual node phenomenon induced by electrophysiological programmed stimulation from hemozygotic rat. (E-H) The atrial effective refractory periods and ventricular effective refractory periods at pacing cycle lengths of 150 ($ERP_{(CL150\ ms)}$) and 120 ms ($ERP_{(CL120\ ms)}$) in the WT, heterozygotic and homozygotic groups. (I-L) Body weight, Wenckebach cycle length (WCL), and atrioventricular node effective refractory periods at pacing cycle lengths of 150 ($ERP_{(CL150\ ms)}$) and 120 ms ($ERP_{(CL120\ ms)}$) in the WT, heterozygotic and homozygotic groups. Data are presented as the mean ± S.E.M.Asterisks indicate statistically significant difference by $P < 0.05$. AVNRT: Atrioventricular nodal reentry tachycardia.

medRxiv preprint doi: https://doi.org/10.1101/2022.03.09.22271906; this version posted March 10, 2022. The copyright holder for this preprint
(which was not certified by peer review) is the author/funder, who has granted medRxiv a license to display the preprint in perpetuity.
It is made available under a CC-BY-NC-ND 4.0 International license .

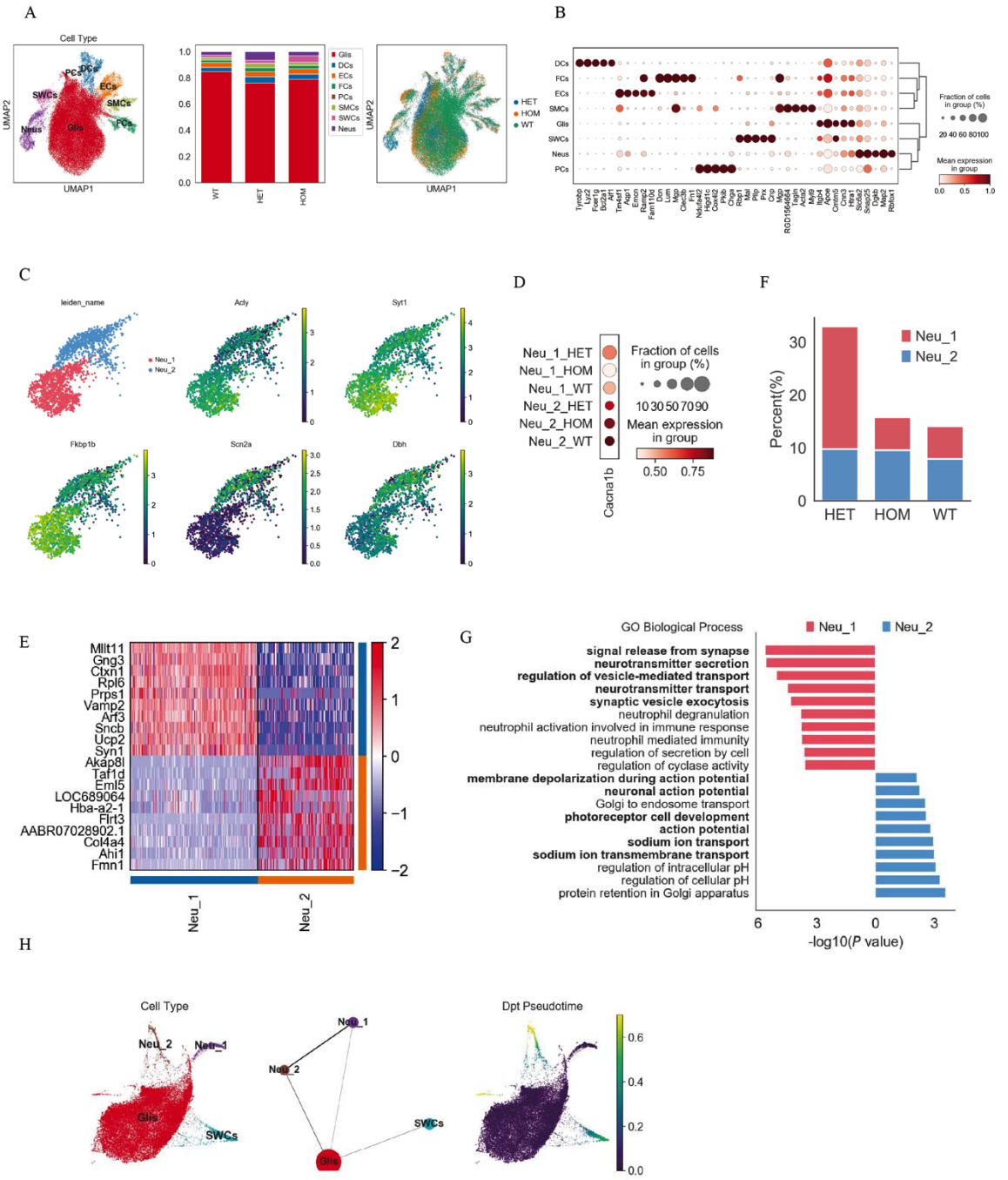

Figure 4. The tSNE plot of single-Cell transcriptomic sequencing, clustering of cells and gene expression profiles in superior cervical ganglion (SCG). (A) SCG cells were assigned cells into 8 different groups. (B) Marker genes were shown in 8 different groups. (C) Neuronal cells were assigned into two subgroups neurons. Some marker genes were shown in two subgroups neurons. (D) Gene expression profile of in two subgroups neurons. (E) Marker genes were shown in two subgroups neurons. (F) The percentage of

medRxiv preprint doi: https://doi.org/10.1101/2022.03.09.22271906; this version posted March 10, 2022. The copyright holder for this preprint
(which was not certified by peer review) is the author/funder, who has granted medRxiv a license to display the preprint in perpetuity.
It is made available under a CC-BY-NC-ND 4.0 International license .

two subgroups neurons was shown in three different rats. (G) The enriched biological process of two subgroups neurons. (H) Pseudotime analysis of two subgroups neurons and other cells.

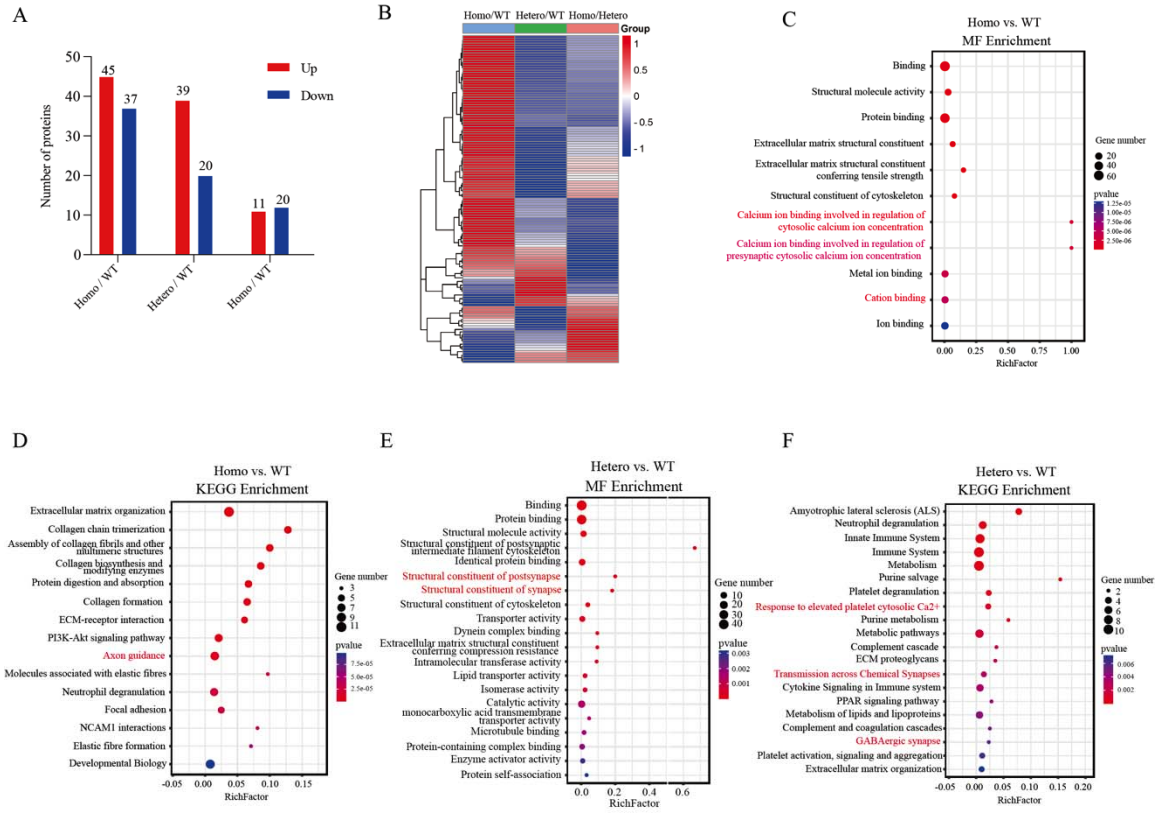

Figure 5. TMT-labeled proteomic analysis of SGC in homozygous and heterozygous rat. (A) Column plots displaying the number of DEPs in the three groups. (B) Heatmap showing the abundance profiles of DEPs in different samples. (C) The molecular function (MF) enrichment in homozygous rat. (D) The KEGG enrichment in homozygous rat. (E) The molecular function (MF) enrichment in heterozygous rat. (F) The KEGG enrichment in heterozygous rat.